2024

The Effect of Ions on the Adsorption of SO2 On a Water Nanoparticle

Nathaniel W. Gillispie

THE EFFECT OF IONS ON THE ADSORPTION OF SO_2 ON A WATER NANOPARTICLE

Nathaniel W. Gillispie

A Thesis Submitted in Partial Fulfillment of the
Requirements for the Degree of
Bachelor of Science with Honors.

Western Kentucky University
May 2024

Abstract

Secondary Organic Aerosols (SOAs) have been of interest to atmospheric chemists for their harmful effects on human health and implications for climate change. Here, we explore a likely system from the early stages of SOA formation. Using computational methods, water nanoparticles with and without ions were simulated. We observe the effects of ions on the adsorption of SO_2 on this system. SO_2 in the atmosphere is associated with greater production of SOAs, so its study is important to SOA formation. We find that the overall structure of water is the most important observable affecting the location of SO_2 within the nanoparticle. Although ions can influence the structure of water, their effect is not as pronounced as the physical constraints of the system itself: the radius of the nanoparticles in this case. We do so by presenting a novel density function based on dipole alignment.

Acknowledgements

I thank the ongoing support of my mentor Dr. Matthew Nee. Without his encouragement and shared interest in research, this thesis would not have been possible. I thank the rest of my committee members, Dr. Jeremy Maddox and Dr. Martha Day, for their support and cooperation. I also acknowledge the WKU High-Performance Computing Center for providing resources that accelerated the progress of this thesis. I greatly appreciate the WKU Honors College and Gatton Academy for providing continued financial support for my studies in relation to this thesis.

Vita

Education

Western Kentucky University 2024

B.S. Chemistry (ACS) with Honors, *Cum Laude*

Gatton Academy of Mathematics and Science 2021

With Honors and Community Scholar distinction

Experience

Student Institutional Researcher 2021 - 2024

WKU Chemistry Tutor 2022 - 2023

Physical Chemistry Teaching Assistant 2024

List of Figures

List of Tables

Contents

1 Introduction

Aerosols are any small solid or liquid pieces of matter dispersed in a gas. Common examples include fog and clouds. For water to spontaneously condense at 25°C, the air must be supersaturated three to four times. Thus, condensation nuclei are virtually required for water to condense into aerosols, even at 100% relative humidity. Gaseous sulfuric acid is one very potent nucleating agent. It is formed in the atmosphere by the photooxidation of sulfur dioxide (SO_2), a relatively abundant atmospheric pollutant.

Aerosols in the atmosphere form in a variety of ways.[1] Naturally, particles made from terrestrial dust and sea spray are called primary aerosols because they are made directly. The kinds of aerosols applicable to this thesis are generated by a coagulation process. These are made from gas-to-particle depositions and are called secondary aerosols. Coagulation can describe the formation of acid rain, smog, and secondary aerosols in general. Also, gaseous organic matter in the atmosphere contributes significantly to the formation of secondary aerosols, so studies often use the term secondary organic aerosol (SOA) to refer to these particles.

As of 1997, the dry mass flux of aerosols from sulfates (derived from SO_2) is about 190Tg per year, the highest among all anthropogenic sources of atmospheric aerosols.[1] This makes the understanding of SO_2 in the context of aerosol formation a discerning goal for those interested in secondary aerosols. It also puts SO_2 in the spotlight of emissions regulations. In 1971, the Environmental Protection Agency established the National Ambient Air Quality Standards to protect human health and the environment, limiting ambient concentrations of SO_2 among other pollutants.[2] From 1980 to 2022, peak daily concentrations of SO_2 decreased by 94% nationally.[3] Despite these advances, SOAs remain a major concern for environmental researchers.

Marti, et. al.[4] have shown that even in rural Colorado, an ideal place to study

the contributions of natural volatile organics, the production of new aerosols tracked more closely with the concentration of SO_2. The production of sulfates, presumed to come from SO_2, was found to be the major driver of new particle formation relative to biogenic sources.

Even in conditions where SOAs are likely to exist without the presence of SO_2, the molecule significantly increases the rate of production of aerosols. Chen, et. al.[5] find that volatile organics from gasoline fumes produce SOAs, but in the presence of SO_2 and NH_3 at typical national levels, SOA production increases from 1.1 - 2.6 times.

Liu, et. al.[6] and Zhao, et. al.[7] both show that the predicted free energy of nucleating atmospheric aerosols is lower when sulfates are involved compared to both water-only and amine-containing scenarios. Nanoparticles consisting of just water tend not to exist past the water cluster phase due to the energetically unfavorable formation process of larger nanoparticles.

Nanoparticles are particles that have a diameter less than 100nm. This is a more general classification that describes the start of the journey of some aerosols. Although all systems simulated here with SO_2 can be classified as aerosols, the term is better reserved for environmental contexts. Nanoparticles, here, simulate the conditions of some freshly nucleated aerosols.

Another interesting factor to explore is ionic strength. Aerosols can undergo concoagulation and evaporation cycles which can create high ionic strength aerosols. In sea spray aerosols, those made by the sloshing of waves in the ocean, the oxidation of SO_2 to sulfate by ozone increases when more sea salt is present in the aerosols.[8] This, of course, leads to a greater overall production of SOAs.

Free radicals in the atmosphere are highly reactive and are of great interest to atmospheric chemists. Hydroxyl radicals, commonly denoted OH, react with SO_2 to form HSO_3 which, in the presence of water, forms sulfuric acid. This reaction can

happen entirely within the gas phase, although the interfacial phase is relevant here. Roeselová et. al.[9] find the OH preferentially binds to the air-water interface while avoiding bulk solution. This thesis then has implications for the production of sulfuric acid in aerosols.

1.1 Motivation

Fine aerosols have direct effects on the human respiratory system. According to The World Bank, "In India, the health cost of outdoor air pollution is estimated at about 1.7 percent of GDP." This is considering the lost work days due to health issues directly associated with pollution. Huang et. al.[10] show that 30-77% of all fine particulate matter ($PM_{2.5}$) produced in strong Beijing smog episodes are SOAs. Chen et. al.[11] showed that in one of Bejing's worst air quality episodes, driven by thick smog and high $PM_{2.5}$ levels, hospital admissions due to cardiovascular disease significantly ($P< 0.05$) increased by 2.27 times. Total hospital admissions also increased significantly by 1.69 times. The understanding of SOA production is important to ambient air quality standards.

Radiative forcing quantifies the change in net radiative flux due to some climate change driver. For example, carbon dioxide increases global temperatures due to positive radiative forcing. Most aerosols, especially sulfur-containing aerosols, have negative radiative forcing effects. This implies SO_2 contributes to climate change but negatively contributes to global warming.

As shown above, the presence of SO_2 is correlated with freshly made SOAs, even though it is not a necessary precursor. In reaction chamber experiments, SO_2 also significantly increases the rate of production of SOAs. Understanding why is an important step in understanding atmospheric chemistry.

1.2 Objective

This thesis seeks to understand how SO_2 interacts with freshly nucleated aerosols. By using molecular dynamics to simulate small nanoparticles, we attempt to fit our results in with the current understanding of ions and the air-water interface. Specifically, we want to understand:

1. Size effects on SO_2 distribution, and similarly, size effects on water structure
2. Ionic effects on SO_2 distribution, and similarly, ionic effects on water structure
3. The effects of different ions

1.3 Overview of Molecular Dynamics

The main experiment of this thesis is entirely computational. One way of classifying computational chemistry methods is either classical or quantum or sometimes a combination of both. Classical simulations that model the motions of atoms using Newtonian dynamics are known as Molecular Dynamics (MD) simulations. This means atoms are modeled as point masses with various interatomic potentials affecting the forces on those atoms. MD simulations don't contain electrons (although sometimes electron density is modeled with massless partial charges), however in quantum calculations, the accurate modeling of electronic behavior is the most pressing task. Quantum calculations are far more complex and computationally intensive making them unfavorable choices for large systems such as these. MD simulations contain explicit bonds which makes the breaking and forming of bonds in MD systems a very challenging topic.

1.4 Thesis Structure

The following chapter discusses molecular dynamics, the choice of simulations for this thesis, and the analysis of the data collected in detail. The next chapter is the

results and discussion containing the main outcomes of the simulations and a guide to understanding their results.

2 Computational Methods

All simulations were performed using the `AMBER14`[12] software suite. Known as Amber, the suite contains over 170 executables designed to prepare, run, and interpret the results of MD simulations. Respectively, `tleap`, `sander`, and `cpptraj` are some executables designed for this. MD simulations are usually classical, meaning the interatomic potentials are based on Newtonian mechanics. Atoms are typically modeled as point masses and point charges, and the potentials between atoms are set at the beginning of each simulation. Newton's laws are applied numerically to advance the simulation. This usually fixes all bonds, preventing chemical reactions.

2.1 The Physics of MD

A force field contains the instructions for calculating the forces that act on individual atoms in MD simulations. It encompasses the collection of parameters describing inter- and intra-molecular interactions for all atom types, as well as the formulas calculating forces given such parameters. In Amber, interactions are modeled classically with several potentials. The potential $U(\mathbf{r})$ of each interaction is directly related to the motion of atoms. In general, force is the negative derivative of potential energy:

$$\mathbf{F} = -\nabla U \tag{2.1}$$

$$\mathbf{a} = \mathbf{F}/m \tag{2.2}$$

From Newton's second law, acceleration $\mathbf{a}_t$ is determined through equation 2.2, and force through 2.1. We want to compute displacement and then add it to the current position $\mathbf{p}_t$ to get the atom position one time-step in the future ($\mathbf{p}_{t+\delta t}$). The second derivative of displacement is acceleration, so acceleration is integrated

twice with respect to time. Theoretically, this procedure is simple, but there are many numerical integration algorithms. In Amber, the SHAKE algorithm uses the Velocity-Verlet algorithm.[13]

Given acceleration and timestep δt, the procedure for updating atom positions is shown in equation 2.3. The current atom velocity is $\mathbf{v}_t$, and the velocity one time-step in the future is $\mathbf{v}_{t+1}$.

$$\begin{aligned} \mathbf{v}_{t+\delta t} &:= \mathbf{v}_t + \frac{\delta t}{2}\mathbf{a}_t \\ \mathbf{p}_{t+\delta t} &:= \mathbf{p}_t + \mathbf{v}_{t+\delta t/2}\delta t \\ \mathbf{v}_{t+1} &:= \mathbf{v}_{t+\delta t/2} + \frac{\delta t}{2}\mathbf{a}_{t+\delta t} \end{aligned} \tag{2.3}$$

The symbol := means the variable on the left side is set to the expression on the right. The procedure is followed for each atom, then the forces are calculated again, then the procedure repeats. Note that the last step in Eq. 2.3 carries the velocity term into the next simulation step when no force is present. This follows from Newton's first law of motion.

Many potentials in Amber are "harmonic": proportional to the square of displacement from some equilibrium position. This term comes from simple harmonic motion, a model used in physics to describe everything from the swinging of a pendulum to the vibrations of molecules. For example, two bonded atoms can vibrate along their bond axis. In Amber, the potential associated with this motion is modeled by $K_b(b - b_0)^2$ where K_b is the bond stretching force constant, b is the bond length and b_0 is the equilibrium bond length. The potential is differentiated analytically to produce a linear expression of force: $F = 2K_b(b - b_0)$. Following Newton's third law, the bond length force acts in an equal but opposite manner to the bonded atoms, for every bond in a simulation.

All forces acting on a molecule can be linearly summed and then integrated when

all forces have been calculated. That is, for any force F_i, the total force acting on the molecule is F_{net}, defined by equation 2.4, the sum of all forces.

$$F_{net} = \sum F_i \tag{2.4}$$

The application of forces to molecules typically takes a small ($< 1\%$) amount of computational time. The calculation of forces spans the overwhelming majority of computational time, necessitating the use of simple yet sufficient forcefields.

2.2 Amber Potential Functions

The Amber force field contains the following total energy potential. Each term represents an interaction from which forces are derived.

$$\begin{aligned} V(r) = & \sum_{bonds} K_b(b - b_0)^2 + \sum_{angles} K_\theta(\theta - \theta_0)^2 \\ & + \sum_{dihedrals} \frac{V_n}{2}\left(1 + cos(n\phi - \delta)\right) \\ & + \sum_{nonbij} \frac{A_{ij}}{r_{ij}^{12}} - \frac{B_{ij}}{r_{ij}^{6}} + \frac{q_i q_j}{r_{ij}} - 2\sum_i \mu_i \cdot \mathbf{E}_{io} \end{aligned} \tag{2.5}$$

The first three terms define the potentials for consecutive two, three, and four bonds. The first term is the bond length potential, involving every two bonded atoms. The second term is a harmonic potential for bond angles θ between all three consecutively bonded atoms. Both terms are shown in the bottom-right of Fig. 2.1. The third term is the sinusoidal potential associated with the interaction between the first and last atoms of a consecutively bonded 4-tuple. Specifically, it acts on the dihedral angle δ between the four atoms. This potential is shown in the top right of Fig. 2.1.

The sum over the "nonbij" term of Eq. 2.5 is for non-bonded interactions. It is known as the Lennard-Jones or 12-6 potential. It acts pairwise for atoms not

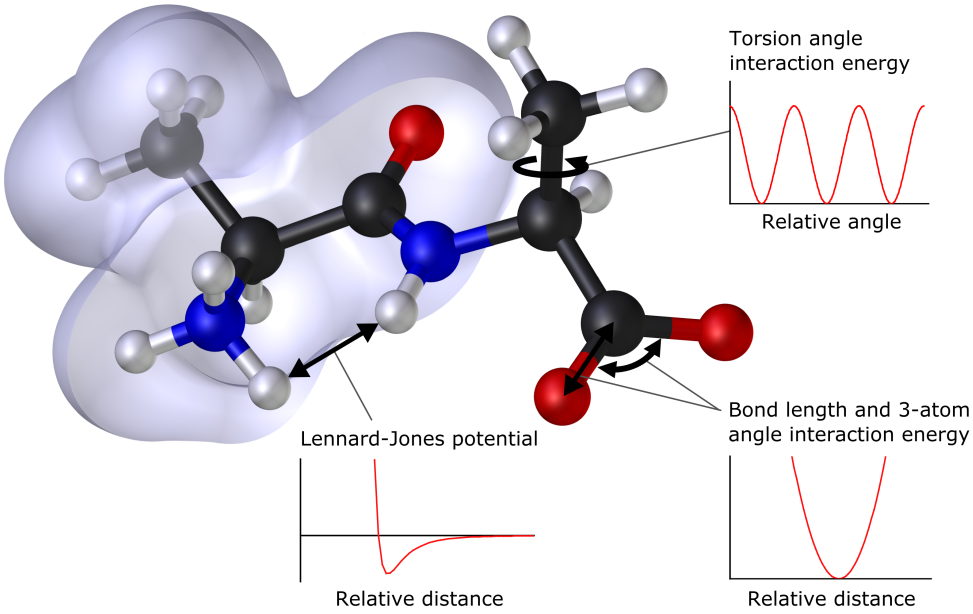

Figure 2.1: Amber's basic forces on an arbitrary molecule. The harmonic potential of bond length and bond angle is shown on the bottom right. Derivative work Dhatfield File:MM PEF 3.png: Edboas, CC BY-SA 3.0, via Wikimedia Commons

connected directly that have distances less than the non-bonded cutoff, generally $\sim$ 10Å. The potential is shown in the bottom center of Fig. 2.1. A more explicit formulation is shown in Eq. 2.6. The terms A_{ij} and B_{ij} are combined terms, being derived from the A_{ii} and B_{ii} terms of atoms i, and A_{jj} and B_{jj} terms of atom j. Amber uses the Lorentz-Berthelot[14] rules for combining A and B parameters. To convert between the AB-form and $\sigma\epsilon$-form, $A = 4\epsilon\sigma^{12}$ and $B = 4\epsilon\sigma^{6}$ for a given atom.

$$
\begin{aligned}
V_{\mathbf{LJ}}(r) &= \frac{A_{ij}}{r_{ij}^{12}} - \frac{B_{ij}}{r_{ij}^{6}} = 4\epsilon_{ij}\left[\left(\frac{\sigma_{ij}}{r_{ij}}\right)^{12} - \left(\frac{\sigma_{ij}}{r_{ij}}\right)^{6}\right] \\
\sigma_{ij} &= \frac{\sigma_{ii} + \sigma_{jj}}{2} \\
\epsilon_{ij} &= \sqrt{\epsilon_{ii}\epsilon_{jj}}
\end{aligned}
\tag{2.6}
$$

The "nonbij" term also includes Coulombic interactions. Partial charges are mod-

eled as point charges at the center of the atom.

2.3 Polarizability

The final term of the Amber force field (equation 2.5) is the polarizable term. Polarizability is a property of a material. It is the propensity for an electric field to induce an electric dipole. In chemistry, this is the common explanation for Van der Waals forces. In MD, this is partially accounted for by the 6-term, or attractive part, of the Lennard-Jones potential. However, Van der Waals forces are highly dependent on the chemical environment, to which the 6-12 potential makes no distinction. MD polarizability provides a correction that helps account for this.

In water, polarizability contributes to its experimental dipole.[15] As such, some water models reduce the partial charges on the atoms by a fixed amount from what would be expected of a non-polarizable model. This amount is set so the total dipole in simulation more closely resembles experiment. This process was used in the POL3[15] model of water and is the basis for assigning polarizabilities and partial charges to SO_2 in the simulations of this thesis. In particular, Caldwell[15] found that reducing the partial charges of molecules by about 89% produced the most accurate dipoles for uncharged polar species.

This is particularly important for simulations involving the air-water interface. Highly polarizable ions in aqueous solution are in higher density at the air-water interface than in bulk solution.[16] This effect is only replicated in MD simulations when polarizability is used.[17] Since we are dealing with the effects of ions in a simulation environment that contains the air-water interface, polarizability is a necessary inclusion.

2.4 Procedure for Simulating Water Nanoparicles

Along with water, many simulations found here contain a unique molecule: sulfur dioxide. The remainder of this section uses SO_2, although the procedure outlined applies to additional uncharged molecules. The problem is that polarizabilities for SO_2 are needed due to the inclusion of the polarizable potential. Non-trivial values were found using the method outlined in Caldwell.[15] Partial charges were defined from quantum mechanical calculations. Using the *Gaussian 09*[18] software package, SO_2 was optimized to an energy minimum using the "CCSD" labeled method with the "aug-cc-pVTZ" labeled basis set. The Mulliken charges from Gaussian multiplied by 0.89 were used for Amber, as described in Caldwell.[15] Equilibrium bond lengths and angles were copied from the optimized Gaussian geometry. The Z-matrix produced by Gaussian for SO_2 explicitly contained these parameters. Van der Waals parameters, bond stretching force constants, and bond angle force constants originated from the Generalized Amber Force Field.[19]

The periodic box was defined with sides $(63 \times 63 \times 63)\text{Å}^3$. This was chosen to fit the largest nanoparticle with at least 25Å plus the diameter of the nanoparticle. Initial configurations were generated using the `packmol` program.[20] The given number of water molecules was placed into a sphere centered at the box center, roughly the coordinates $(32, 32, 32)$Å. SO_2 was placed at the origin, outside the aerosol to avoid close contact. For the simulation with ions, water molecules were removed at random and replaced using `tleap`. The VdW interaction cutoff was set to 10Å and the simulation timestep to 1fs. For each simulation, the following steps were performed.

First, the box was minimized for 1000 steps using the SHAKE algorithm to ensure bond lengths don't change over minimization.[13] Second, the box was heated from 0K to 300K using the Langevin thermostat. Third, the box was equilibrated twice for 200ps each at 300K. The ensembles for equilibration were NPT and NVT respectively.

Lastly, a production run lasting 500ps was performed at 300K with the NVT ensemble. The analysis is described in the Analysis section.

The NPT equilibration step is not necessary at all and is an artifact from previous simulations. There is a possibility that the box size shrinks to remove the vacuum surrounding the nanoparticle given enough time. In practice, 0.2ns is not enough simulation time to induce more than a negligible 0.5Å change in box size.

The POL3 water model was used. This was chosen because it is a polarizable form of the TIP3P model, which we were previously using. Polarizability is a crucial parameter as discussed in the previous section.

Table 2.1 contains the atomic forcefield parameters.

Atom	Mass (amu)	q(e^-)	LJ σ	LJ ϵ	α(Å^3)
O	16.0	-0.730	1.798	0.156	0.528
H	1.008	0.365	0	0	0.170

Parameter	Equilibrium state	Potential (kcal/mol)
O-H bond	1.0Å	365
H-O-H angle	109.47°	535

Table 2.1: Force field for water. α is the isotropic polarizability.

Table 2.2 contains a list of all simulations for this thesis. Simulations, or simulation runs, are also simply called "runs."

We chose these simulations to test the following:

1. Size effects on SO_2 distribution, and similarly, size effects on water structure
2. Ionic effects on SO_2 distribution, and similarly, ionic effects on water structure
3. The effects of different ions

Thus, the main variables here are the size of the nanoparticle, the quantity and type of ions, and the presence of SO_2. The size effects of water were tested by simulating water-only nanoparticles of various sizes. To test the size effects on SO_2 distribution, the same simulations were repeated after replacing a single water molecule

Name	N(H_2O)	N(SO_2)	N(Na^+)	N(Cl^-)	N(NH_4^+)	N(SO_4^{2-})
12	12	0	0	0	0	0
36	36	0	0	0	0	0
101	101	0	0	0	0	0
226	226	0	0	0	0	0
376	376	0	0	0	0	0
SO2_11	11	1	0	0	0	0
SO2_35	35	1	0	0	0	0
SO2_100	100	1	0	0	0	0
SO2_225	225	1	0	0	0	0
SO2_375	375	1	0	0	0	0
SO2_2NaCl_371	371	1	2	2	0	0
SO2_7NaCl_361	361	1	7	7	0	0
SO2_16NaCl_343	343	1	16	16	0	0
SO2_2NH42SO4_369	369	1	0	0	4	2
SO2_7NH42SO4_354	354	1	0	0	14	7

Table 2.2: All simulations. The left column contains the name of the runs. The subsequent columns are how many molecules of a species there are.

with an SO_2 molecule. The simulations testing ionic effects took the above simulation containing 375 water molecules, replacing water molecules with ions as needed. This procedure was completed randomly before the start of the simulation using the `tleap` program. To test these variables, analysis must be done after the simulations.

2.5 Analysis

MD simulations allow the study of the classical motion of molecules at a femtosecond timescale. Practically, this is done when frames of the simulation are saved at regular intervals. In our case, the final equilibrated state of the system was studied. The 500ps production run was used for analysis. This thesis investigates the orientation of water within an aerosol and how ions affect the solvation of SO_2. To accomplish this, we observe two main distribution functions.

The first is the radial distribution function, abbreviated as RDF and commonly notated $g(r)$. This can be obtained from experimental neutron scattering data, providing another link between computation and experiment. In Amber, this function

can be calculated using the `cpptraj` program.

Second, we also observe the radial dipole correlation density function (RDCDF or $d(r)$)[†]. This likely does not correlate to a physical measurement, but is useful in demonstrating structure, as will be shown.

The RDF gives the density of a species some radius from a given point. If that given point is set to be the oxygen atom on water, for example, we get the classic pair distribution function of water, a special case of the RDF which can be obtained from neutron scattering experiments. In our case, we set the given point to be the center of mass (COM) of the nanoparticle. According to the Amber14 Reference Manual:[12]

> The RDF is calculated from the histogram of the number of particles found as a function of distance R, normalized by the expected number of particles at that distance. The normalization is calculated from
>
> $$Density * \left(\left[\frac{4\pi}{3}(R + dR)^3 \right] - \left[\frac{4\pi}{3} dR^3 \right] \right) \tag{2.7}$$
>
> where dR is equal to the bin spacing... The default density value is 0.033456 molecules Å^{-3}, which corresponds to a density of water approximately equal to 1.0g mL^{-1}.

This is useful in showing where molecules are in the simulation, specifically where the interface is, and where SO_2 is most likely to be relative to the center of the nanoparticle.

The RDCDF operates similarly, but rather than the density of molecules, we look at the density of dipole correlation. Assuming a spherical interface, it is a way of observing how correlated dipole moments are to the interface closest to them. In the case of nanoparticles, we assume the interface takes the shape of a sphere centered at the center of mass of the nanoparticle. The vector extending from the center of mass of the nanoparticle to an arbitrary molecule has the same direction as the normal vector on the interface closest to that molecule. The normal vector of this sphere is sufficient to describe the interface, both its location and direction. The density

[†]This notation is likely new.

function is calculated in a manner similar to Eq. 2.7. Given two vectors $\mathbf{u}$ and $\mathbf{v}$, the angle θ between them is given by

$$\cos\theta = \frac{\mathbf{u}\cdot\mathbf{v}}{\|\mathbf{u}\|\|\mathbf{v}\|} \tag{2.8}$$

The $\cos\theta$ value is calculated through Eq. 2.8. The two vectors $\mathbf{u}$ and $\mathbf{v}$ are the dipole moment of a molecule and the vector generated by subtracting the position of the center of mass of a given molecule and the COM of the nanoparticle. A visual explanation of this angle is found in Fig. 2.2. If, for a given distance from the center of mass of the nanoparticle, molecules are uniformly randomly rotated, the RDCDF should be zero. However, if there is a non-zero value in the RDCDF, on average there is a dipole moment aligned radially for a given distance from the COM.

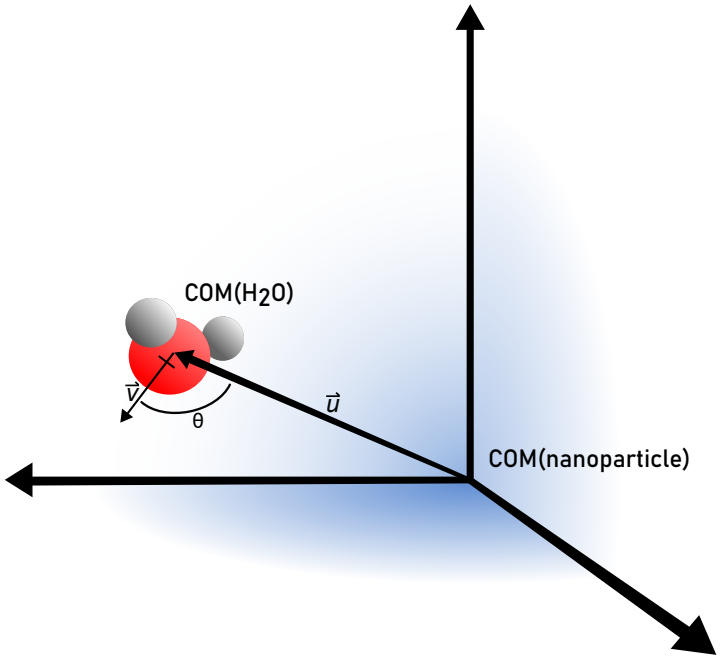

Figure 2.2: A visual explanation of the $\cos\theta$ calculation. Vector $\mathbf{u}$ is directed away from COM(nanoparticle) towards COM(H_2O). Vector $\mathbf{v}$ is the dipole moment of water. θ is the angle between $\mathbf{u}$ and $\mathbf{v}$.

In our testing, the histogram bin size that produced the best results for the amount

of data collected was 0.05Å. Since the density functions are normalized to volume, the magnitude of the RDCDF should only be due to dipole alignment, sparing wild fluctuations in radial density. That is, if there are no dipoles, there cannot be dipole alignment, thus, no RDCDF. Although it would be possible to normalize RDCDF to radial density, in testing, this was not found to be as useful; and outside the interface, indeterminate expressions become likely.

3 Results and Discussion

It is important to establish a benchmark to observe the effects of ions on water nanoparticles. The formation of small water clusters around SO_2 has been studied.[21,22] Water inside carbon nanotubes and other cylindrical structures, as well as "slab" structures has been well documented.[23] Different geometries of confinement and sizes of water particles are abundant in the literature. However, water nanoparticles, particularly of sizes found here, are less studied but occupy an important transitory space for aerosol chemistry. Water particles of diameter 1-4nm are transitory in the sense that water in the bulk mode begins to emerge. They are also transitory in that they are too large for theoretical quantum treatment, but too small to be physically collected by particle impactors. Finally, they are often literally transitory. Even at elevated relative humidity levels, water nanoparticles of the sizes studied here can be regarded as transition states between dispersed molecules and the nucleation mode of an aerosol.[7]

We claim that the bulk mode of water emerges at the nano-scale. This is theoretically explained with geometry. The surface area of a sphere is proportional to the radius squared while the volume is proportional to the radius cubed. As radius increases, water molecules are more likely to be within a water nanoparticle than on it. Another size effect comes from the nature of spheres. The curvature of a sphere is the inverse of the radius squared. As radius increases, curvature decreases until the limit at infinity: the sphere resembles a plane. This means at a sufficiently large radius, the behavior on the surface of a water nanoparticle should mimic that of a slab of water with sufficient depth.

3.1 Water Nanoparticles

Water nanoparticles alone exhibit ordered structures when observed radially. This is seen in both the radial density functions and the previously described radial dipole correlation density functions. For 226 water molecules, both functions can be found in Fig. 3.1.

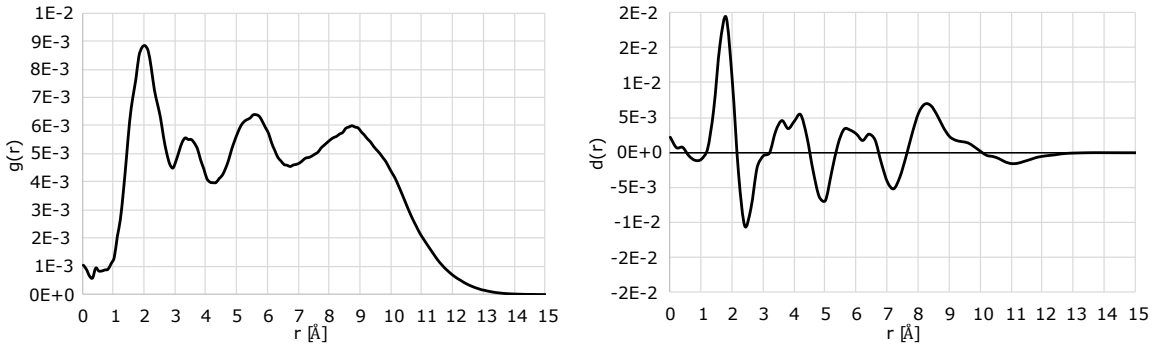

Figure 3.1: RDF and RDCDF for 226 water molecules. On the left is the RDF and on the right is the RDCDF. There is a clear oscillatory pattern present in both functions. Notice the last peak in RDCDF. This peak corresponds to interfacial water and will be compared to simulations containing different numbers of water molecules.

According to the RDF, there is some non-zero density of water from the center of mass to 10.4Å away, but the density approaches zero at greater radii. This should be expected from water nanoparticles.

In the RDCDF plots, there are a series of oscillations but importantly, there is a negative peak at 11Å, where the interface should be. In general, this feature is seen in all RDCDF plots for each simulation. This feature means that on average, hydrogen atoms are further from the center of the nanoparticle than their corresponding oxygen atoms. In other words, the hydrogen atoms point outwards. This effect is noted by other researchers by probing the surface of water with sum frequency generation spectroscopy, they noted a more specific situation where OH groups point inwards.[24]

Although present in all air-water interfaces, the extent of this effect is a function of nanoparticle size. The intensity of the last $d(r)$ minimum in each water-only

simulation is plotted with the radius at which the peak occurs in Fig. 3.2.

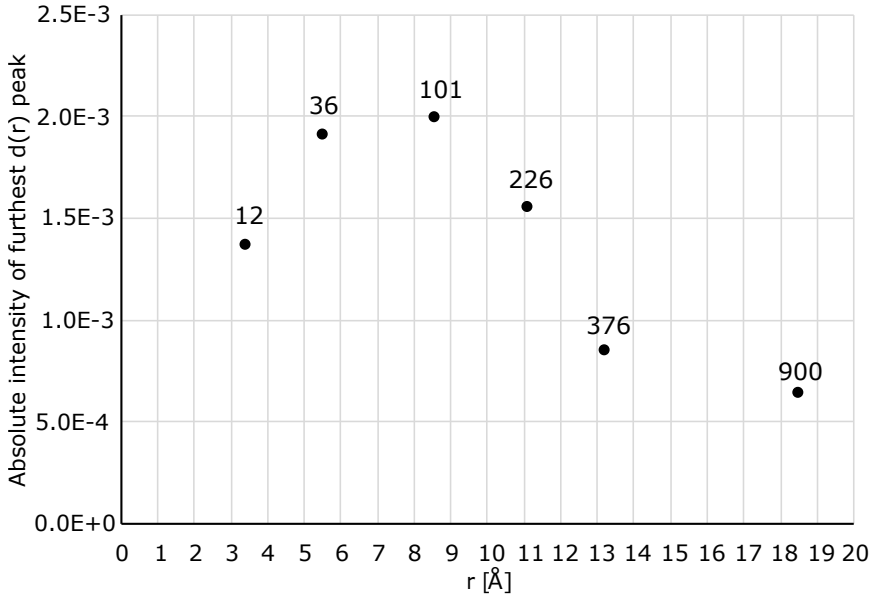

Figure 3.2: Plot of absolute intensity of the radially furthest $d(r)$ peak for water-only runs.

In the limit of large nanoparticles, experimental data suggests this effect remains,[24] implying asymptotic behavior. Previous literature has stressed the importance of surface hydrogen bond networks to water's ability to solvate gas phase molecules.[25] Theoretically, then, nanoparticle size should be an important factor in the solvation of SO_2.

It should be noted that the intensity of the last peak of $d(r)$ is not necessarily an indicator of hydrogen bonding at the air-water interface. As will be discussed, smaller water-only nanoparticles are more likely to solvate SO_2 in bulk than larger ones. This most likely has to do with the bulk structure of water, not just interfacial water. To demonstrate, the RDCDF of the interfaces of three water-only runs is shown in Fig. 3.3 along with the full RDCDF of the same runs.

When in the context of the whole RDCDF, the final peaks representing the orientation of the water at the interface seem static in comparison (which isn't the case as seen in Fig. 3.2). Clear oscillatory structures appear in the dipole correlation of

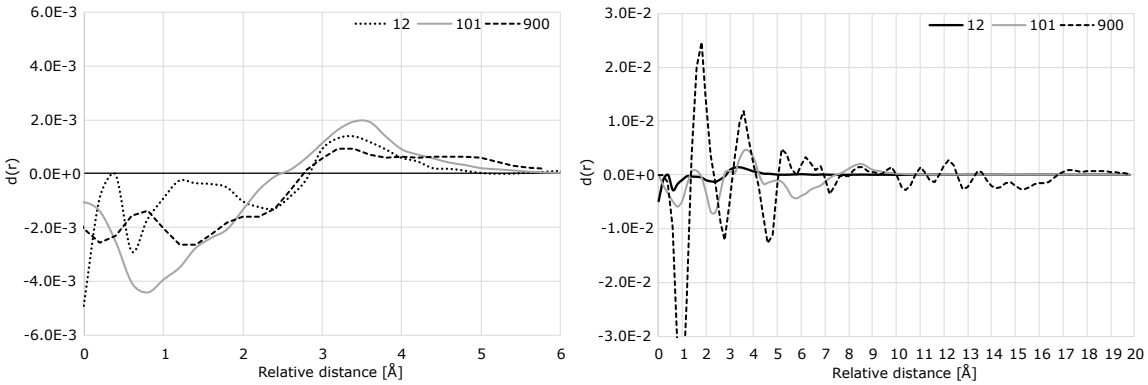

Figure 3.3: On the left is a visual comparison of the RDCDF at just the interface for the 12, 101, and 900 molecule runs. The right contains the entire RDCDF function to scale. Notice the final peaks at around 3, 8, and 18Å.

nanoparticles as size increases. This pattern only intensifies near the center of the nanoparticle, or rather, away from the interface when the bulk mode appears. The original claim that bulk-mode water appears as aerosol size increases is supported by this data.

One fundamental problem with RDCDF is that it does not imply an underlying structure like hydrogen bonds. In fact, Liu et. al.[26] show that near the interface of air and water, the proportion of water molecules engaging in hydrogen bonding is higher than in the aqueous phase. This is likely because water molecules translationally diffuse faster at the interface and can easily orient into more energetically favorable states. This might explain why water solvates ions at the interface quickly. Irudayam and Henchamn[25] show the strong ability of halides to accept a single hydrogen bond over water. What remains unexplained is why the solvation of SO_2 is slow, despite SO_2 being highly soluble in water. That is why adsorb SO_2, but not absorb it?

3.2 Water and Sulfur Dioxide

The `SO2_WAT`[†] type runs observe what happens to water nanoparticles upon replacing a single water molecule with a SO_2 molecule. In most runs, SO_2 remains on

[†]Refer to Table 2.2 for the names of each run.

the edge of the aerosol. See Fig. 3.4 for the most likely radius of SO_2 plotted against the nanoparticle size. An exception has been made for peaks occurring below around 3Å as some plots were noisy in this range due to less data.

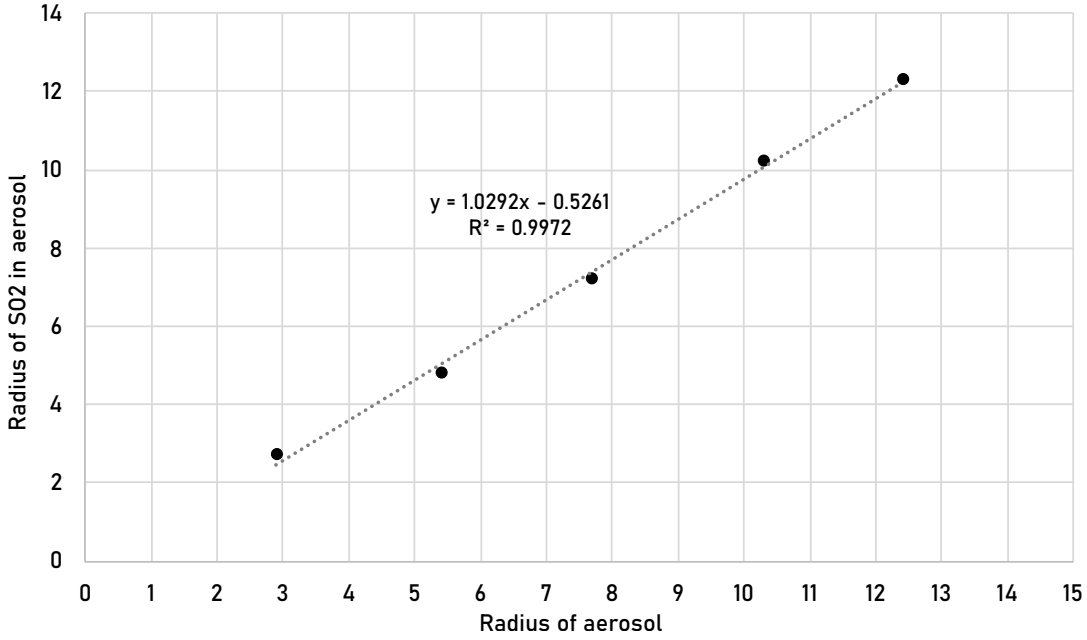

Figure 3.4: Correlation of most likely SO2 position to the interface of water only runs. A linear trend is observed. This corresponds to SO_2 remaining on the interface.

The correlation between the interface and the most likely position of SO_2 is very linear. It is known that SO_2 adsorbs to the air-water interface.[27] So this should be expected.

Although SO_2 remains on the interface regardless of nanoparticle size, a look into the full RDF of SO_2 tells a different story. The plots in Fig. 3.5 show the RDFs for all species in the water and sulfur dioxide simulations. There is a clear shift in the distribution of SO_2. In smaller particles, the molecule spends time within the inner part of the nanoparticle. There is some non-zero density of SO_2 near the center of the nanoparticle for `SO2_11` and `SO2_35` runs. As size increases, this turns into zero density near the center.

The translational advantage of interfacial water may cause the water within a

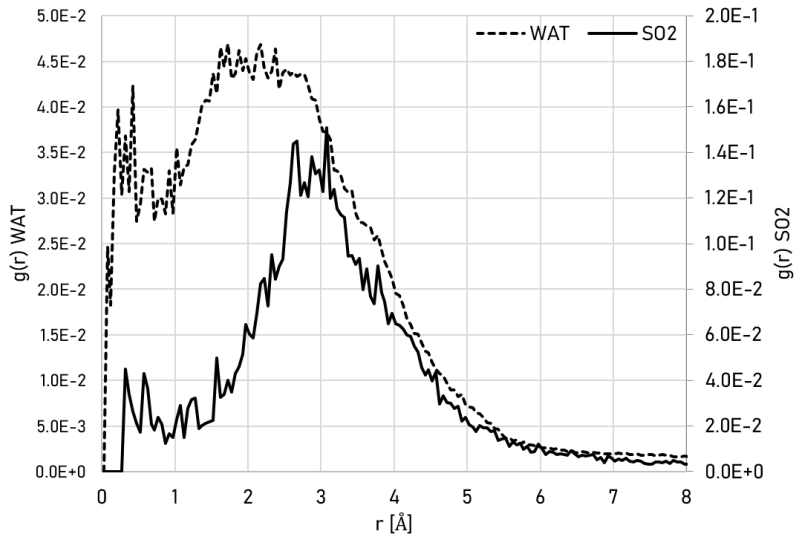

Figure 3.5a: SO2_11 RDF.

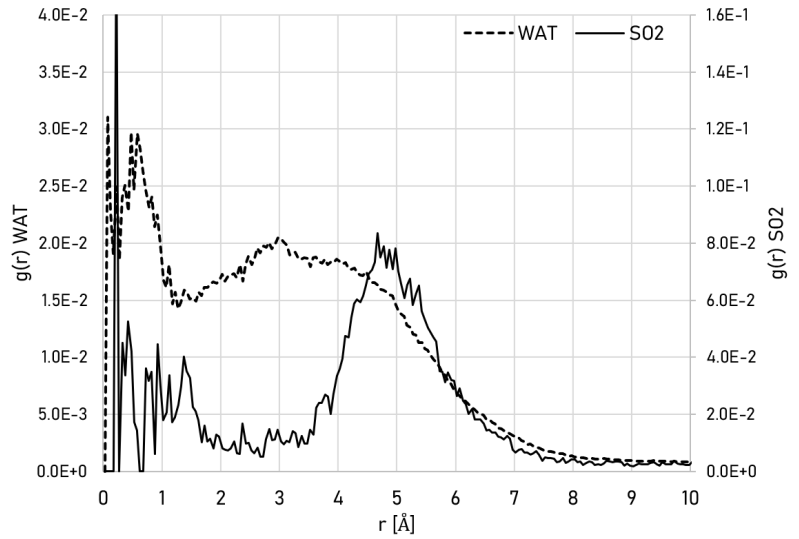

Figure 3.5b: SO2_35 RDF.

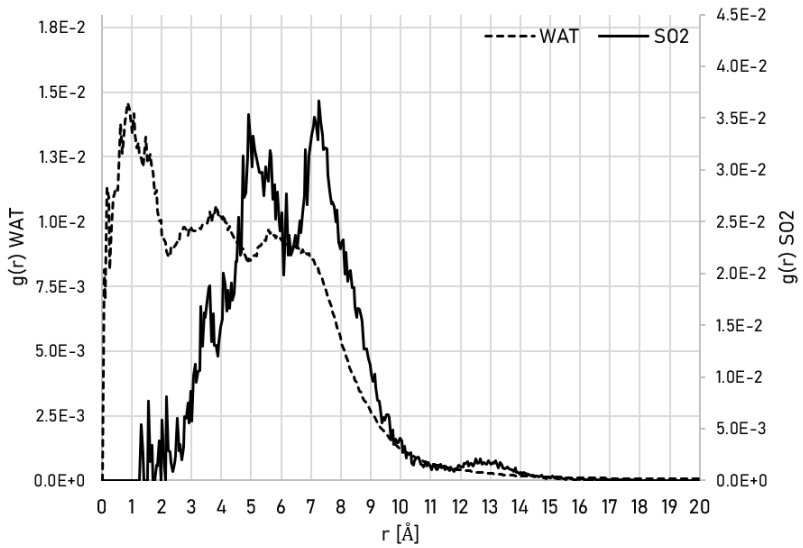

Figure 3.5c: SO2_100 RDF.

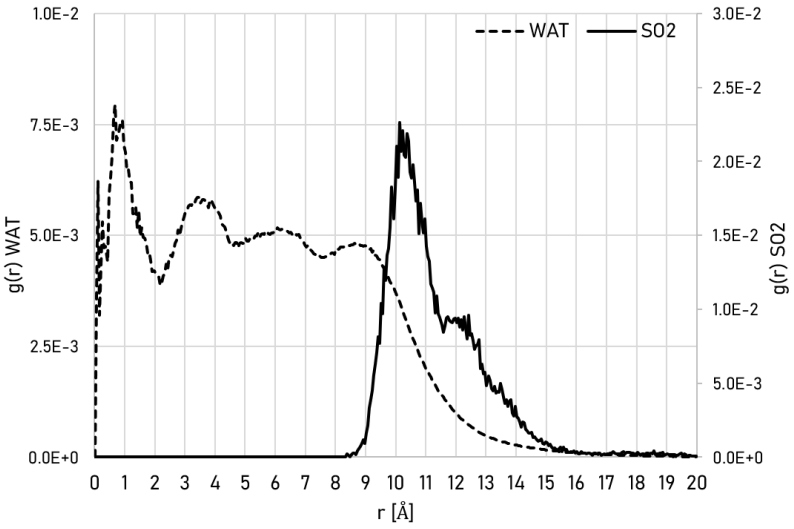

Figure 3.5d: SO2_225 RDF.

nanoparticle to "conform" to the interface. This is consistent with the idea that there are more hydrogen bonds proportional to water molecules at the interface versus bulk. Because larger nanoparticles have more volume, the bulk water has more space to arrange into strong hydrogen bond networks. Assuming hydrogen bonds are the strongest interactions that contribute to the solvation of SO_2, Fig. 3.5 suggests hydrogens are more likely to bond with SO_2 in smaller aerosols. Hydrogen bonds are typically only broken in aqueous solution when there is another hydrogen bond that forms as a result.[25] If smaller aqueous nanoparticles engage in less hydrogen bonding proportional to their mass, this would explain the solvation of SO_2 only in those nanoparticles, as well as the energetic barrier water nanoparticles face when forming.[7] To test this, we now look at ions.

3.3 The Case With Ions

Ions disrupt the structure of pure water. They can be labeled kosmotropes or chaotropes when they induce order or disorder, respectively, to the structure of water.[28] The Hofmeister series orders some ions on their kosmotropic properties.[29] Ammonium sulfate is not only involved in atmospheric chemistry reactions, but both its ionic constituents also rank highly in the Hofmeister series. Sodium and chloride appear as mid-range ions in the series, with a kosmotropic propensity far below that of ammonium sulfate[†]. Leroy et. al.[30] provides the perspective that chaotropic ions are adsorbed at the interface, and kosmotropic ions are absorbed into bulk. If this is true, we would expect sodium chloride in one simulation to exist closer to the interface than ammonium sulfate in another. Fig. 3.6 gives the RDFs of the simulations with two molecules of each ion.

In reality, the difference between the locations of ions with just four ions over 500ps

[†]There is some debate about the ranking of ammonium against sodium ion. The Hofmeister series for cations is less established. Some rankings place ammonium highly, some place it equal to sodium ion, and some place it below sodium ion.

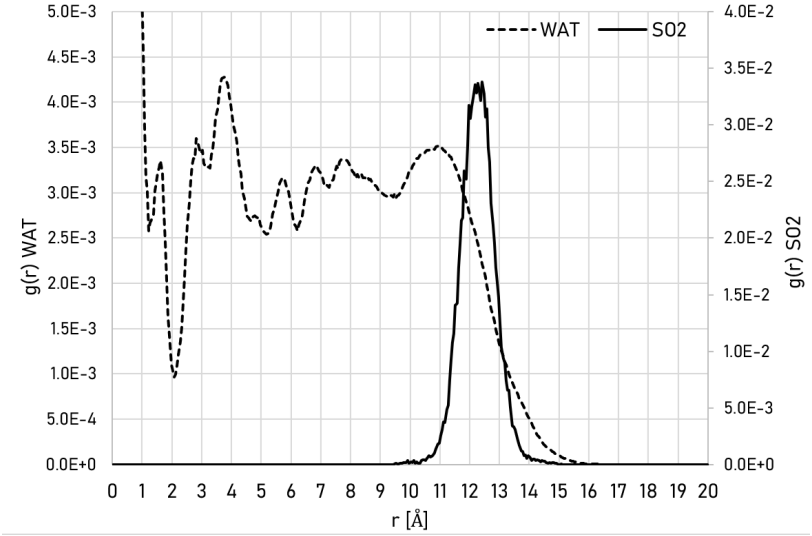

Figure 3.5e: From top to bottom :`SO2_11`, `SO2_35`, `SO2_100`, `SO2_225`, and `SO2_375` RDF. Note that as the nanoparticle increases in size, the distribution of SO_2 within the molecule narrows relative to the radius until at 375 H_2O, the distribution resembles a Gaussian one. As mentioned, there are higher peaks in the `SO2_35` RDF, but these are excluded due to noise.

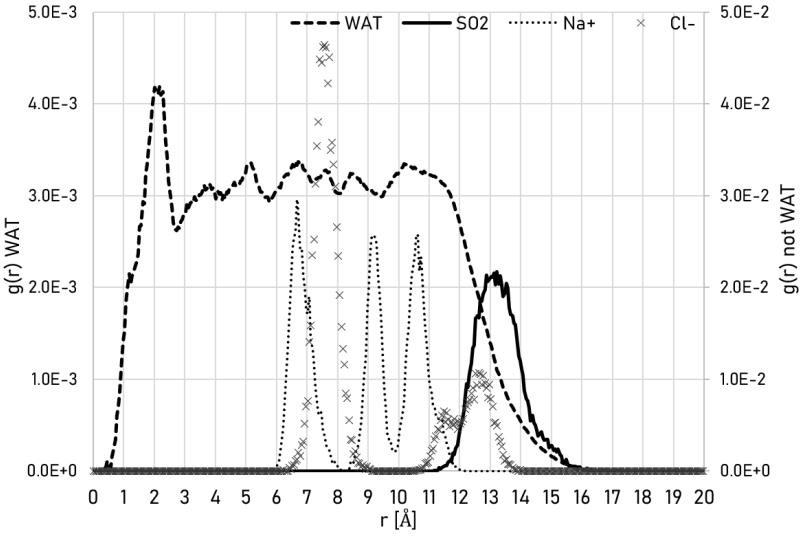

Figure 3.6a: `SO2_2NaCl_371` RDF.

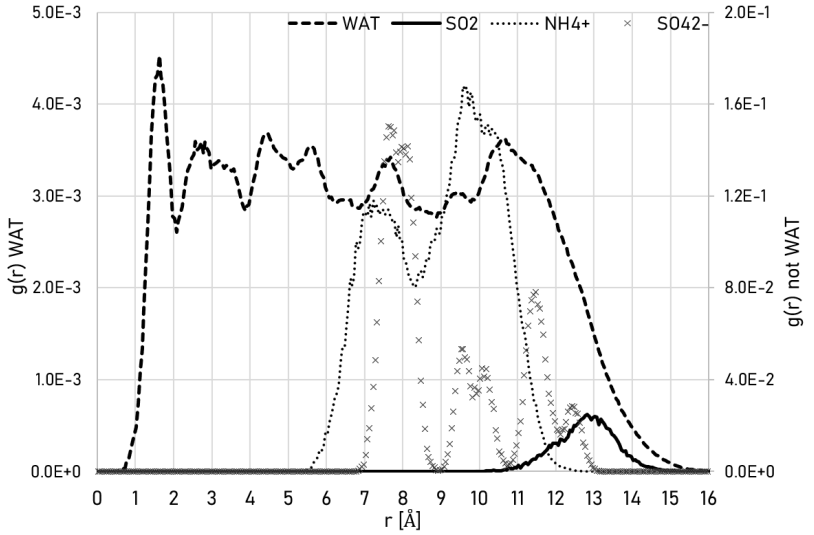

Figure 3.6b: `SO2_2NH42SO4_369` RDF. With only two atoms of each ion, no noticeable changes are made. Compared to the runs without ions, SO_2 is radially further out. Notice the multiple ionic peaks. These migrations had no large energetic differences according to Amber.

of simulation time cannot be visually detected. This NaCl simulation corresponds to a concentration of about 0.3M.

For the simulations with seven molecules of each ion, the concentration of NaCl corresponds to an approximate 1M concentration. In Fig. 3.7, there is a visual difference in the locations of ions. Although the location of ammonium sulfate within its simulation more closely corresponds to a Gaussian distribution, the sodium chloride simulation appears multimodal. Sodium ion exists in bulk at a radius of 7Å, but also closer to the interface in a cluster approximately centered at a radius of 11Å. Chloride appears in two bimodal clusters approximately centered at 5 and 12Å. For the ammonium sulfate run, ammonium appears in a cluster at a radius of 9Å and sulfate appears in a cluster centered around 9Å too. When observing the interfacial clusters, indeed, NaCl resides closer to the interface. Radially, SO_2 is sandwiched between the sodium and chloride ions.

Theoretically, we expect the SO_2 molecule to orient itself in alignment with the ions. This is due to the dipole of SO_2 aligning with the dipole generated by the

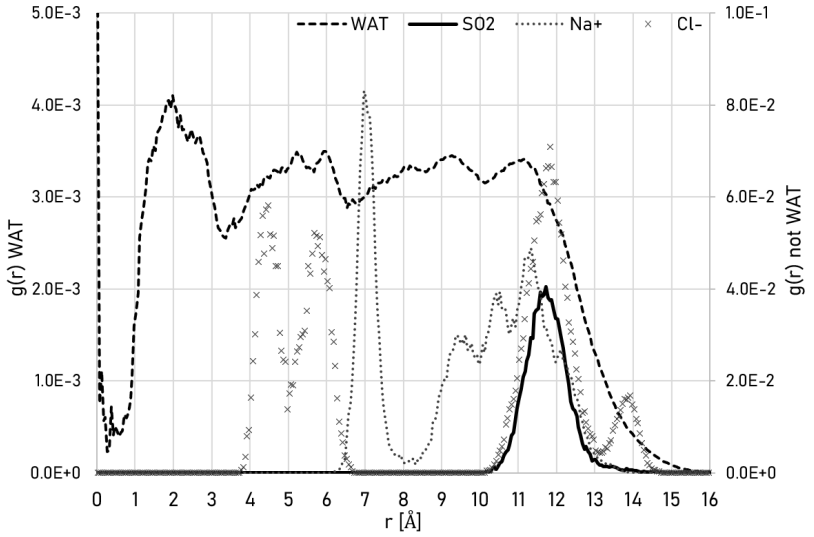

Figure 3.7a: `SO2_7NaCl_371` RDF.

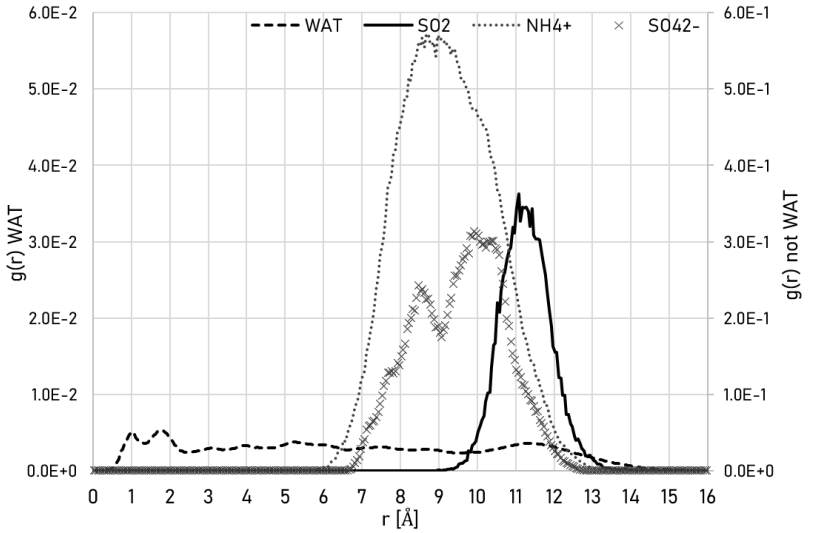

Figure 3.7b: `SO2_7NH42SO4_369` RDF. Notice the bulk of ammonium sulfate is away from the aerosol as expected from kosmotropic agents.

separation of positively and negatively charged ions. In fact, even without ions, this should be possible. Electric fields at the air-water interface are estimated to be up to $\sim 1 \times 10^8$V cm^{-1}.[31]

In Fig. 3.8 we observe a dipole moment aligned with the interface. However, if we look at the ammonium sulfate case in Fig. 3.9, we observe the same effect with a similar intensity. The peak $d(r)$ value for the sodium chloride run is about -0.00014. For ammonium sulfate, the peak $d(r)$ value is -0.00016, and for the no ion case it is -0.00017, found in Fig. 3.10. Peak $d(r)$ measurements may not be as effective as an integral over the entire distribution function, but at least it demonstrates that ions are not that effective at inducing a radial dipole in SO_2 compared to the interfacial water on its own. From this perspective, the ions don't affect the solvation of SO_2

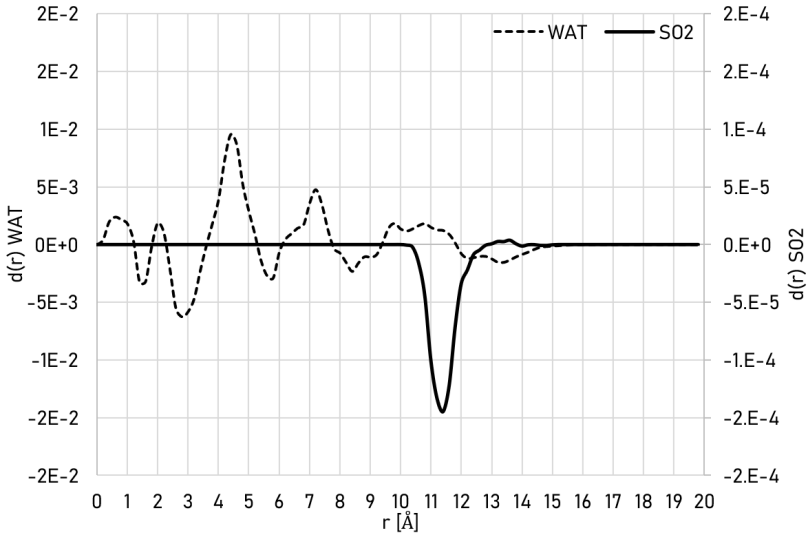

Figure 3.8: `SO2_7NaCl_361` RDCDF.

In Fig. 3.4, we saw the location of SO_2 relative to the water surface. Now, we will look at the same measure as applied to the ionic runs. Fig. 3.11 contains the most likely location of SO_2 plotted against the radius of the nanoparticle for every ionic run.

In the smaller concentrations, SO_2 is found further from the center of the aerosol. This cannot be due simply to the size of the aerosol increasing. If that were the case,

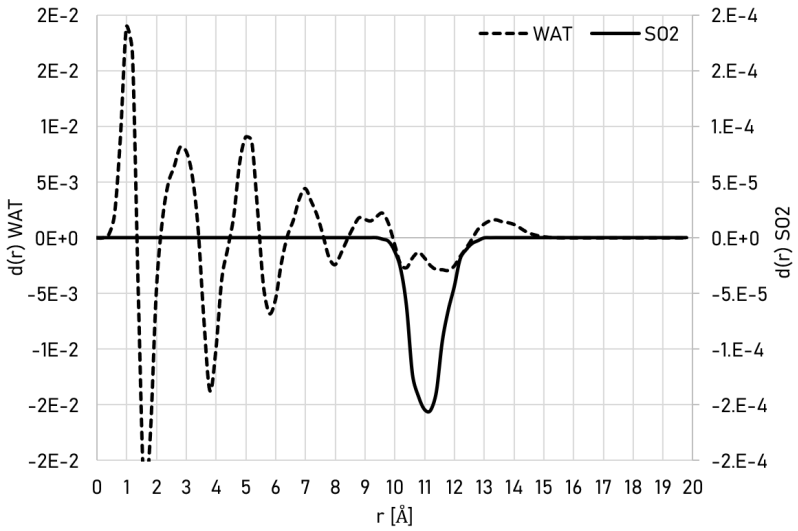

Figure 3.9: `SO2_7NH42SO4_354` RDCDF. Observe the highly kosmotropic effects of ammonium sulfate as it induces highly radially ordered structures in water.

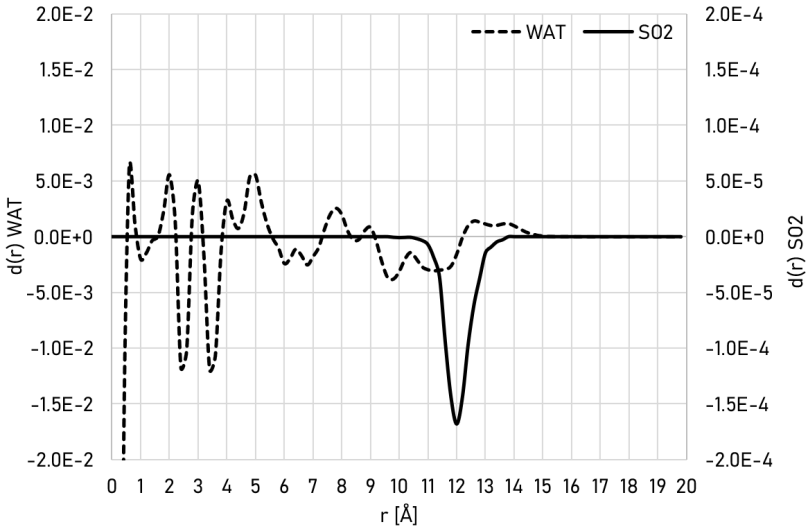

Figure 3.10: `SO2_375` RDCDF.

we would find all the ionic runs following the same trendline set by the non-ionic runs. Something unique happens with ions that move SO_2 relative to the interface. In the more concentrated ionic runs, the radius of SO_2 decreases.

Clearly, ions affect the structure of water, changing the location of SO_2 relative to the interface, but not in an easily measurable way. The RDCDF plots suggest that ions do not affect the radial dipole of SO_2, however, the RDF plots show a clear

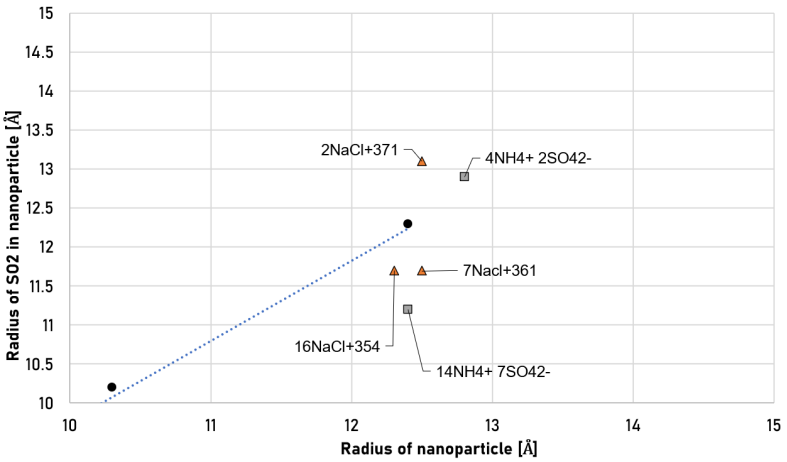

Figure 3.11: Most likely location of SO_2 plotted against the radius of the nanoparticle for every ionic run. The trendline is for the non-ionic simulations.

difference between ion-containing nanoparticles and nanoparticles without ions.

4 Conclusion

In the second chapter, we set out to test three things:

1. Size effects on SO_2 distribution, and similarly, size effects on water structure
2. Ionic effects on SO_2 distribution, and similarly, ionic effects on water structure
3. The effects of different ions

In the previous chapter, we saw that based on the radial dipole of SO_2, ionic nanoparticles are indistinguishable from non-ionic nanoparticles. However, considering the radial density of SO_2, there is an observable difference between ionic and non-ionic nanoparticles. Compared to nanoparticles with no ions, adding small concentrations initially extrudes SO_2 radially outwards, then brings SO_2 inwards towards bulk solution in higher concentrations. This is not to say that ions do not affect the dipole of SO_2, but that the radial shift of SO_2 within a nanoparticle is not due to the dipole generated by the separation of positively and negatively charged ions. It must be due to the change in the structure of water itself.

The structure of water within and on the surface of nanoparticles is highly dependent on size, as shown in Fig. 3.2. In Fig. 3.5 we saw that smaller, less organized nanoparticles were more likely to solvate SO_2 in the bulk. However, we did not see this effect to nearly the same extent when looking at the radial distribution of SO_2 for ion-containing nanoparticles.

Taken together, we can conclude that ions influence the structure of water in a non-trivial way. But, the physical constraints of the water system itself, radius in our case, have a larger effect on water structure than ions (up to about 1M) which then affects the adsorption of SO_2.

One question that remains is the utility of the RDCDF function. It provides a quantifiable value to the observed effect of water orientation at the air-water interface, which is typically visually hard to detect. Also, it implies radial structure within water. Although this does not correspond to a single observable such as dipole alignment at the interface, it is a known fact that water forms hydrogen bond networks. This alone does not necessitate a radial structure but provides a good explanation for the oscillations seen in RDCDF plots of pure water nanoparticles. More testing on well-known systems is needed to determine any further utility of the RDCDF.

Considering that OH radicals prefer the air-water interface, likewise with SO_2, the air-water interface of nanoparticles, or freshly nucleated aerosols, provides a good space for these compounds to mingle and react. Unfortunately, the study of the most important aerosols in this case, those with the highest surface area, are too large to be simulated here. The surface area distribution of SOAs peaks at 1000Å in radius,[1] is far larger than the radii of nanoparticles simulated here. Statistically, gas-phase molecules in the atmosphere are far more likely to land on these larger aerosols than the freshly nucleated aerosols simulated here. More research is needed to fully understand the implications of interfacial reactions.

4.1 Advice to Future Computationalists

Checkpoint files have two main formats: NetCDF and ASCII. The former is to be preferred in almost all circumstances. NetCDF stores checkpoints in a compressed format containing atom coordinates, velocities, cell lengths, and so on. Commands `ncdump` and `ncgen` can be used to interconvert NetCDF to human-readable ASCII and back. It may be useful to restrain atoms using the restraint force and then give the atoms a "push" by altering the velocities in the checkpoint file.

In Amber, simulation parameters are found in an ".mdin" file and include variables like temperature, pressure, periodic boundary conditions, and the length of the

simulation. The positions of molecules are found in input coordinates (".inpcrd") files or from the output (restart or ".rst") of other simulations. The list of molecules and their forces are found in parameter topology (".prmtop") files which `tleap` generates.

When Amber parallelizes orthographic simulations, it cuts the simulation box into 'slabs' in the xy-plane. When running multiphase simulations, or those with large changes in density, the axis with the greatest variation in density should be either the x or y axis so that a similar number of atoms are in each slab. The data presented in this thesis simulates a spherical aerosol. In this case, there is no dimension which results in an equal distribution of atoms in the xy-slabs. Therefore, parallelization causes instability.

Various combinations of processors and nodes should be tested to determine the optimum settings for parallelization of a given simulation. In our system, the optimum settings were one node running the maximum number of processors.

We recommend using aliases for common commands. For example, the `qsub` command, used to submit jobs, includes options to send an email when the job halts. Aliasing `qsub -m [youremail]` as `qsube` for example, may be useful. `wq` may be aliased for `watch qstat -n 2` which displays the output of `qstat`, refreshing every two seconds. The Linux `~/bash.rc` file is where these aliases can be defined.

In Amber14 there is no single command which "turns on" the force field. Three things should be done to do so. First, in `tleap`, the line `set default IPOL 1` should be included. Second, polarizabilities of each atom type should be included after the mass definition in the Amber parameters file(s), in units of $Å^3$. Third, when saving `prmtop` and `inpcrd` files, the command `SaverAmberParmsPol` should be used rather than `SaveAmberParms`. Note that `pmemd` does not support the polarizable forcefield as of Amber14.

The `mdinfo` file is created in the directory specified by the file submitted with the job, known as the `pbs` file. It contains information written to the `mdout` file appended

with the timing information, for example, nanoseconds of simulation time per day of real-time and time remaining. It may be useful to use the command `tail -f mdinfo` to see the file as it updates every ntpr simulation steps.

In general, it should be assumed that programs have unexpected behaviors. Test all the edge cases you can imagine; the developers haven't thought of everything.

Bibliography

(1) Seinfeld, J. H.; Pandis, S. N., *Atmospheric Chemistry and Physics: From Air Pollution to Climate Change*, 1st edition; Wiley-Interscience: Hoboken, NJ, 1997, p 102.

(2) Definition of National Ambient Air Quality Standards (NAAQS) `https://ohioepa.custhelp.com/app/answers/detail/a_id/907/~/definition-of-national-ambient-air-quality-standards-(naaqs)` (accessed 04/25/2024).

(3) US EPA Sulfur Dioxide Trends `https://www.epa.gov/air-trends/sulfur-dioxide-trends` (accessed 04/25/2024).

(4) Marti, J. J.; Weber, R. J.; McMurry, P. H.; Eisele, F.; Tanner, D.; Jefferson, A. *Journal of Geophysical Research: Atmospheres* **1997**, *102*, 6331–6339.

(5) Chen, T.; Zhang, P.; Chu, B.; Ma, Q.; Ge, Y.; He, H. *Environmental Science & Technology* **2023**, *57*, 6616–6625.

(6) Liu, L.; Guo, S.; Zhao, Z.; Li, H. *The Journal of Physical Chemistry A* **2022**, *126*, 2407–2416.

(7) Zhao, Z.; Kong, K.; Wang, S.; Zhou, Y.; Cheng, D.; Wang, W.; Zeng, X. C.; Li, H. *The Journal of Physical Chemistry Letters* **2019**, *10*, 1126–1132.

(8) Yu, C.; Liu, T.; Ge, D.; Nie, W.; Chi, X.; Ding, A. *Environmental Science & Technology* **2023**, *57*, 6609–6615.

(9) Roeselová, M.; Vieceli, J.; Dang, L. X.; Garrett, B. C.; Tobias, D. J. *Journal of the American Chemical Society* **2004**, *126*, 16308–16309.

(10) Huang, R.-J. et al. *Nature* **2014**, *514*, 218–222.

(11) Chen, R.; Zhao, Z.; Kan, H. *American Journal of Respiratory and Critical Care Medicine* **2013**, *188*, 1170–1171.

(12) D.A. Case; V. Babin, J.T. Berryman, R.M. Betz, Q. Cai, D.S. Cerutti, T.E. Cheatham, III, T.A. Darden, R.E. Duke, H. Gohlke, A.W. Goetz, S. Gusarov, N. Homeyer, P. Janowski, J. Kaus, I. Kolossváry, A. Kovalenko, T.S. Lee, S. LeGrand, T. Luchko, R. Luo, B. Madej, K.M. Merz, F. Paesani, D.R. Roe, A. Roitberg, C. Sagui, R. Salomon-Ferrer, G. Seabra, C.L. Simmerling, W. Smith, J. Swails, R.C. Walker, J. Wang, R.M. Wolf, X. Wu and P.A. Kollman Amber 14, University of California, San Francisco, 2014.

(13) Ryckaert, J.-P.; Ciccotti, G.; Berendsen, H. J. C. *Journal of Computational Physics* **1977**, *23*, 327–341.

(14) Song, W.; Rossky, P. J.; Maroncelli, M. *The Journal of Chemical Physics* **2003**, *119*, 9145–9162.

(15) Caldwell, J. W.; Kollman, P. A. *The Journal of Physical Chemistry* **1995**, *99*, 6208–6219.

(16) Jungwirth, P.; Tobias, D. J. *The Journal of Physical Chemistry B* **2002**, *106*, Publisher: American Chemical Society, 6361–6373.

(17) Wick, C. D.; Kuo, I.-F. W.; Mundy, C. J.; Dang, L. X. *Journal of Chemical Theory and Computation* **2007**, *3*, 2002–2010.

(18) M. J. Frisch; G. W. Trucks, H. B. Schlegel, G. E. Scuseria, M. A. Robb, J. R. Cheeseman, G. Scalmani, V. Barone, B. Mennucci, G. A. Petersson, H. Nakatsuji, M. Caricato, X. Li, H. P. Hratchian, A. F. Izmaylov, J. Bloino, G. Zheng, J. L. Sonnenberg, M. Hada, M. Ehara, K. Toyota, R. Fukuda, J. Hasegawa, M. Ishida, T. Nakajima, Y. Honda, O. Kitao, H. Nakai, T. Vreven, J. A. Montgomery, Jr., J. E. Peralta, F. Ogliaro, M. Bearpark, J. J. Heyd, E. Brothers, K. N. Kudin, V. N. Staroverov, R. Kobayashi, J. Normand, K.

Raghavachari, A. Rendell, J. C. Burant, S. S. Iyengar, J. Tomasi, M. Cossi, N. Rega, J. M. Millam, M. Klene, J. E. Knox, J. B. Cross, V. Bakken, C. Adamo, J. Jaramillo, R. Gomperts, R. E. Stratmann, O. Yazyev, A. J. Austin, R. Cammi, C. Pomelli, J. W. Ochterski, R. L. Martin, K. Morokuma, V. G. Zakrzewski, G. A. Voth, P. Salvador, J. J. Dannenberg, S. Dapprich, A. D. Daniels, Ö. Farkas, J. B. Foresman, J. V. Ortiz, J. Cioslowski, and D. J. Fox Gaussian 09, Wallingford CT, 2009.

(19) Wang, J.; Wolf, R. M.; Caldwell, J. W.; Kollman, P. A.; Case, D. A. *Journal of Computational Chemistry* **2004**, *25*, 1157–1174.

(20) Martínez, L.; Andrade, R.; Birgin, E. G.; Martínez, J. M. *Journal of Computational Chemistry* **2009**, *30*, 2157–2164.

(21) Steudel, R.; Steudel, Y. *European Journal of Inorganic Chemistry* **2009**, *2009*, 1393–1405.

(22) Dermota, T. E.; Hydutsky, D. P.; Bianco, N. J.; Castleman, A. W. *The Journal of Physical Chemistry A* **2005**, *109*, 8254–8258.

(23) Xue, M.; Hu, Z.; Qiu, H.; Shen, C.; Guo, W.; Zhang, Z. *National Science Review* **2022**, *9*, nwab214.

(24) Nihonyanagi, S.; Mondal, J. A.; Yamaguchi, S.; Tahara, T. *Annual Review of Physical Chemistry* **2013**, *64*, 579–603.

(25) Irudayam, S. J.; Henchman, R. H. *The Journal of Chemical Physics* **2012**, *137*, 034508.

(26) Liu, P.; Harder, E.; Berne, B. J. *The Journal of Physical Chemistry B* **2005**, *109*, 2949–2955.

(27) Donaldson, D. J.; Guest, J. A.; Goh, M. C. *The Journal of Physical Chemistry* **1995**, *99*, 9313–9315.

(28) Moelbert, S.; Normand, B.; Rios, P. D. L. Kosmotropes and chaotropes: modelling preferential exclusion, binding and aggregate stability, 2004.

(29) Gregory, K. P.; Elliott, G. R.; Robertson, H.; Kumar, A.; Wanless, E. J.; Webber, G. B.; Craig, V. S. J.; Andersson, G. G.; Page, A. J. *Physical Chemistry Chemical Physics* **2022**, *24*, 12682–12718.

(30) Leroy, P.; Lassin, A.; Azaroual, M.; André, L. *Geochimica et Cosmochimica Acta* **2010**, *74*, p. 5427.

(31) Liu, Y. et al. *Chem* **2024**, *10*, 330–351.